EXECUTIVE SUMMARY

IDENTIFICATION AND ANALYSIS OF MEO OBSERVATION STRATEGIES FOR A FUTURE EUROPEAN SPACE SURVEILLANCE SYSTEM

A. Vananti, A. Hinze, T. Schildknecht

Version 1.0

Bern, September 2011

Main Contractor: Astronomical Institute of the University of Bern, Switzerland (AIUB)
Sub-Contractors: THALES ALENIA SPACE, Toulouse, France
DEIMOS SPACE S.L., Madrid, Spain
ESA Study Manager: H. Krag

ESA Contract 21599/08/F/MOS

DOCUMENT CHANGE RECORDS

Version	Date	Changes
Draft 0.0	Sep. 2011	Initial draft
Version 1.0	16.09.2011	Final Version

LIST OF CONTENTS

LIST OF ABBREVIATIONS

AIUB	Astronomical Institute of the University of Bern
AMR	Area-to-Mass Ratio
CCD	Charge Coupled Device
DISCOS	Database and Information System Characterising Objects in Space
ESA	European Space Agency
ESASDT	ESA Space Debris Telescope
FOV	Field Of View
GEO	Geostationary Earth Orbit
GTO	Geostationary Transfer Orbit
MJD	Modified Julian Date
ODPS	Online/Offline Data Processing System
OGS	Optical Ground Station (ESA)
RAAN	Right Ascension of the Ascending Node
SNR	Signal-to-noise Ratio
ZIMSMART	Zimmerwald Small Aperture Robotic Telescope

1 INTRODUCTION

The largest part of the mass launched into space actually becomes 'space debris' or 'orbital debris' immediately after launch. Upper stages, payload shrouds, adapter rings are left in near Earth space. After the accomplished mission even the payload will become space debris eventually. The estimates, such as made using ESA's reference model MASTER, give a total of about 150 million space debris objects larger than 1 millimeter in 2005. These smaller space debris objects stem from many different sources. For object sizes larger than 1 centimeter, fragments generated by explosions of satellites and spent upper stages or by collision events are dominating the environment in most orbital regions. The increasing number of space debris objects creates an increasing threat to manned and unmanned space missions, ranging from temporary system outage to the loss of the control over the spacecraft. Beside space debris mitigation measures and some "natural" effects that clean-up some orbital regions, the only way of dealing with the space debris threat is the continuous observation of the space debris environment. Today, larger space debris objects are in fact routinely tracked by means of ground-based (and to a small extent also by space-based) sensors, while the threat from smaller space debris objects is assessed using space debris environment models. While active satellites can be maneuvered in order to avoid collisions with the tracked space debris objects, reference models of the space debris population allow spacecraft designer and mission operators to include effective measures in the planning and operation phase of space missions. However, the development and validation of models of the space debris environment relies on the availability of (at least statistical) orbit information of the space debris objects. Space debris can only be detected with optical telescopes when the space debris objects are illuminated by the Sun while the sky background is dark. Contrary to optical telescopes, radars can be operated during daytime and nighttime, at all weather conditions. The big advantage of telescopes over radars, however, resides in their higher sensitivity in terms of object size at large distances.

The space debris population in the low Earth orbit (LEO) region, which is defined as the region up to 2000 kilometers altitude, has been extensively studied during the last decade and reasonable models covering all size ranges were produced. Information on the distribution of objects in the geostationary ring (also called geostationary Earth orbit, GEO) and the geostationary transfer orbits (GTOs), however, is still comparatively sparse. Recognizing the paramount importance of protecting the GEO from contaminating space debris, ESA initiated an optical search for fragments in the GEO to improve the knowledge about its debris population and to understand the future evolution of this population. These optical observations are performed with ESA's Zeiss 1 meter telescope located at the Teide Observatory at Tenerife, Spain. The search campaigns were highly successful and detected a large number of debris objects in GEO, in GTO, and a in a wide range of high-altitude orbits [RD-9], and led to the detection of a new class of space debris objects (objects with high area-to-mass ratios) [RD-10][RD-11]. First observations took place in autumn 1999 and regular space debris surveys have been performed since January 2001.

An extension of the ongoing space debris surveys to new orbital regions, in particular to the increasingly populated medium Earth orbit (MEO) region, is the logical next step. The space debris environment in the MEO region has not been systematically investigated so far and is

thus largely unknown. A corresponding survey program will obviously strengthen ESA's leadership in optical observations of space debris in high-altitude orbits.

2 OBSERVATION STRATEGIES

The observation of man-made objects in near-Earth space is usually distinguished between two missions: "space surveillance" and "space debris measurements". The first mission combines all tasks needed for building up and maintaining a complete catalogue of orbital elements of all objects larger than a specific size in a defined spatial volume. The second mission denotes research projects focusing on the acquisition and interpretation of data describing the characteristics of space debris objects in a given survey volume in a more statistical manner. Space debris surveys must be designed such that they yield a statistically well-defined sample of the (small-size) space debris population in a given orbit region. The most important optimization parameter when searching for space debris is the sensitivity to detect small-size objects that requires "blindly" tracking the sensor with the expected apparent motion of the objects of interest. It was decided to concentrate the analysis during this study in terms of "space debris measurement", rather than "space surveillance". One of the main hardware constraints using the ESA Space Debris Telescope (ESASDT) at the Optical Ground Station (OGS) for surveys is its relatively small field of view (FOV) of 0.7°. The limited FOV not only reduces in general the area covered during the observations, but also makes difficult the detection of moving MEO objects. The ESASDT processing software bases on the masking technique, which requires series of frames of the same inertial (declination/right ascension) field. The absolute minimum of number of frames is two, but ideally they should be three or more to reduce false alarm rate due to cosmics, without need for filtering angular velocity and inclination. If we assume a MEO object angular velocity of about 30"/s, the dwell time in the FOV is around 84 s. With cycle (read/slew) time of 18 s this translates into an average of 4.2 frames per tracklet. Depending on the position of the satellite the velocity may vary from 26"/s up to 38"/s. These high angular velocities require blind tracking of the observed object during the exposure.

2.1 MEO survey strategies

2.1.1 MEO population

As input for the generation of the reference population the DISCOS catalogue (epoch 54986 MJD) was used. A refined MEO definition was used, focusing on the objects with mean motion between 1.5 and 2.5 and eccentricity smaller than 0.2. The results comprise 214 objects in various classes: GPS satellites (Block I and II), GLONASS satellites, rocket bodies (3rd stages, 4th stages, Apogee motors), and others (other satellites, debris). Most of the objects are in near-circular orbits. For the GPS satellites, there are two groups distinguishable: the older Block-I with a widespread distribution of semi-major axis and the newer Block-II in a band comparably narrow to the GLONASS. Block I satellites orbit with about 63° inclination and the most of them are at about 250° right ascension of the ascending node (RAAN). For the Block-II one may easily recognize 6 orbital planes around 55° inclination, equidistantly placed over the full right ascension range at 36°, 96°, 156°, 216°, 276°, and 336°. The

GLONASS satellites are grouped in three orbital planes at about 65° inclination and 43°, 163°, and 283° RAAN. The GLONASS population is accompanied by a larger part of the rocket bodies population. In conclusion, from these first considerations, coverage of the inclination band between about 50° and 70° could be appropriate.

2.1.2 Explosion model

In order to identify possible debris clouds due to explosions in the MEO region, a set of fragmentations has been simulated, taking into account a reasonable range of ejection velocities as a function of the fragment size. For the breakup model we have referred to the study of Pardini and Anselmo [RD-2] and the cumulative number of fragments as a function of the diameter is shown in Figure 2-1.

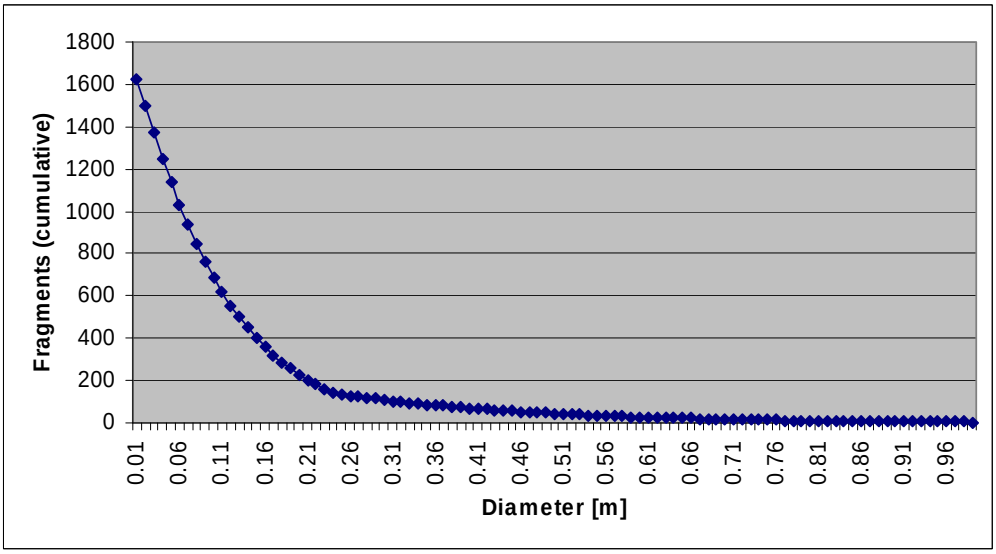

Figure 2-1: Cumulative number of fragments as a function of the diameter

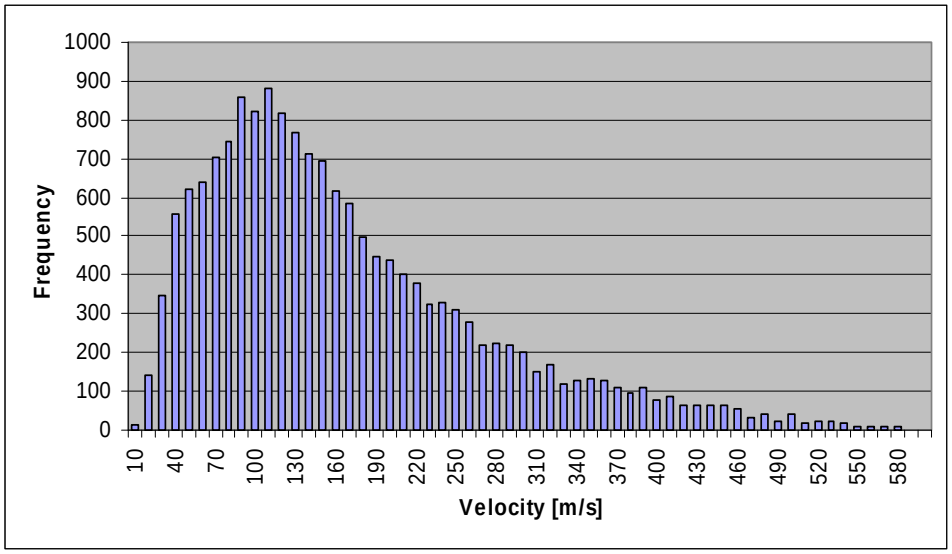

Figure 2-2: Distribution of the ejection velocities

The velocity of the ejected fragments as a function of the diameter combined with the number of fragments results in the distribution of the ejection velocities shown in Figure 2-2. The maximal number of fragments is reached at about 100 m/s. In the explosion model an isotropic ejection of the fragments was assumed. According to the above velocity distribution, randomly oriented velocity vectors were added to the original velocity of the exploded object. The culmination point and the ascending node were selected as representative locations along the orbit for the explosion. Due to the explosion the orbit of the fragments will differ from the original orbit. GPS and GLONASS orbits were taken into account and the distributions of the single orbital elements after the explosions were calculated. As a consequence of the explosion the semi-major axis distribution is broadened around the value of the original orbit with a deviation of about 1000 km. The excentricity distribution exhibits a peak around 0.03. All the fragments show a more excentric orbit than the one of the parent object, with a broad range of values between 0.01 and 0.1. The inclination and RAAN also exhibit a clear scattering. The analysis of the orbital elements also shows that the argument of perigee and, after few complete orbits, the mean anomaly are homogeneously distributed.

Since a fragmentation event can occur to each of the MEO objects in the reference catalogue, the next step consists in applying the explosion dispersion to the distribution of the reference population. The convolution of the two distributions was calculated for all orbital elements. In the excentricity the dispersion due to the explosion is predominant, whereas in the ascending node the width is mostly characterized by the existing population distribution. The semi-major axis and the inclination data have an approximate Gauss distribution. A best fit with a Gaussian function yields a standard deviation σ_a = 1200 km and σ_i = 1.5° for the semi-major axis and the inclination, respectively.

In order to study the evolution of the synthetic explosion population we referred to the "Detailed assessment of a European Space Surveillance System" study [RD-1]. In the latter the ephemeris propagation capabilities of the program SATORB contained in the CelMech software [RD-3] were used and a propagation duration covering ~55 years was applied. The analysis of the evolution indicates that the semi-major axis remains constant over the whole period. The inclination varies with a certain periodicity but the relative values do not diverge: satellites starting with similar inclination keep similar values over longer intervals. The motion of the ascending node is about -14°/year for Block-II and slower with about -11°/year for Block-I satellites. The nodes are in relatively narrow bands at the beginning of the simulation, but evolve to cover larger ranges during the considered time. The eccentricity of the orbits may grow up to 0.08 in the next 30 years, but this is strongly dependent on the initial eccentricity. For satellites starting with an eccentricity of 0.03 a growth of up to 0.16 is possible. Based on the indications given by the evolution model, a statistical relevant measure for the dispersion of the synthetic fragments population was examined. The RAAN of the active population of GPS and GLONASS satellites between 2006 and 2009 was analyzed. The resulting deviation in the RAAN is σ_{RAAN} = 5°. The average deviation from the initial excentricity value was extrapolated after 15 years and a value of σ_{exc} = 0.01 was determined.

The explosion distribution was convoluted with the evolution dispersion after 15 years. The total standard deviation is composed by the explosion and evolution deviations: $\sigma^2_{tot} = \sigma^2_{expl} + \sigma^2_{evol}$. In Table 2-1 are summarized the values for semi-major axis, excentricity, inclination, and RAAN. A synthetic population of 1000 objects was generated using Gaussian distributions with these dispersions and with the centers at the average orbital elements of different subgroups in the reference population. The subgroups were chosen according to the current 6

average orbital planes of the GPS constellation and the 3 orbit planes of the GLONASS one. Additionally one average orbit representing some of the GPS Block I satellites was selected.

Description	σ expl.	σ evol.	σ tot.
A [km]	1200	~ 0	1220
e	0.02	0.01	0.022
i [°]	1.5	0.5	1.6
RAAN [°]	5	5	7

Table 2-1: Summary of the deviations in the orbital elements

2.1.3 Survey region definition

Based on the synthetic population generated in the previous subsection different observation regions were evaluated. We consider a field with given right ascension α and declination δ. This field is crossed by all orbits with inclinations i equal to or larger than $|\delta|$ and ascending node Ω that fulfills the equation:

$$\sin(\alpha - \Omega) = \tan(\delta) \cot(i).$$

In the (Ω, i) space the latter equation defines a stripe of finite width depending on the FOV of the optical sensor. All the objects, with planes whose (Ω, i) combination falls within the stripe, cross the FOV of the sensor pointed in the direction (α, δ). In Figure 2-3 the poles corresponding to the orbital planes of the objects in the synthetic population are represented on a gnomonic projection. The azimuth identifies the RAAN Ω and the radial scale indicates the inclination i. In this representation the stripes are delimited by straight parallel lines. The covered field is identified with the normal to the stripe through the center of the diagram. The azimuth of the normal line and the radius, from the center up to the stripe, are directly related to the (α, δ) field. It is relative easy to guess from the diagram the possible observation fields. There are four possibilities for the GPS population indicated in Figure 2-3, other combinations are equivalent but considering other population clouds. A similar analysis can also be done for the GLONASS population. The four fields taken into account are:

- Right ascension: 96°, Declination: 0°
- Right ascension: 66°, Declination: 35.5°
- Right ascension: 96°, Declination: 51°
- Right ascension: 66°, Declination: 55°

It is possible to roughly estimate the relative coverage, only in terms of crossing events, from the geometrical intersection between the two-dimensional Gaussian population distribution in the (Ω, i) plane and two parallel planes perpendicular to the (Ω, i) plane and parallel to the considered stripe. But in order to achieve a more accurate estimation it is necessary to perform simulations with a realistic model. In the following sections, the results of performance simulations using the ESA Program for Radar and Optical Observation Forecasting (PROOF) [RD-4] are presented.

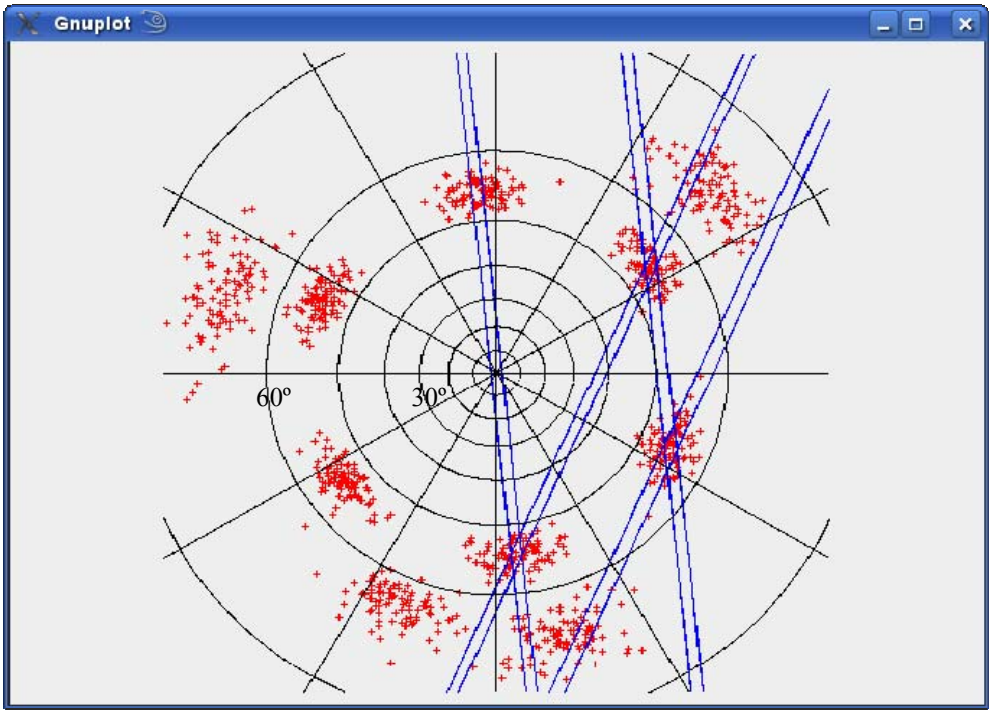

Figure 2-3: Poles of orbit planes of the synthetic population (gnomonic projection)

2.1.4 Coverage and correlation

In the previous paragraph the optimal observation regions were discussed, in order to achieve high detection rates of objects belonging to a hypothetical explosion population. However, to exhaustively cover a certain sky region during a period, the observation strategy needs to consider the FOV of the sensor and the dwell time of MEO objects in the given FOV. If the dwell time is much larger than the time needed for an observation cycle (exposure, readout, new telescope pointing), an area bigger than the FOV can be covered without missing any object passing in the meantime. A sequence of adjacent observations, according to the FOV, forms a so-called fence. The concept of leak-proof is used if all objects, given a limiting size, passing the fence are detected. For a successful orbit determination more than one observation tracklet is necessary. Subsequent tracklets can be obtained either with tasked follow-ups for a specific object or, in a survey-only strategy, with the combination of difference fences. The observations in the fences need to be correlated for a successful orbit determination. The constraints for a leak-proof strategy with two or more fences depends essentially on the FOV of the telescope and on the exposure cycle time. As mentioned before, the ESASDT has a FOV of 0.7° and a cycle time of 18 s. This makes it difficult to conceive a reasonable fence strategy and only a single field strategy applies, with the considerations described in the previous paragraph.

In view of possible observations with the ZimSMART telescope in Zimmerwald, different strategies have been analyzed. The FOV of ZimSMART is 4.2° and the cycle time is 17 s. A MEO object with a velocity of 30”/s stays in the FOV around 500 s. Three main survey scenarios were conceived with two vertical declination stripes with a difference of about 15° in right ascension, around the culmination region. The scenarios have stripes with 7, 5, and 3

fields, respectively. The fields have a slight vertical overlap of 0.4°. The sequence of fields in the stripe (stripe cycle) is observed several times. Also, for every field several frames are acquired. In the scenario with 7 and 5 fields, a number of 4 and 5 frames per field allow 4 stripe cycles to be executed during about 30 minutes. After that, to catch the objects detected in the first stripe, 8 cycles in the second stripe are assumed. In the scenario with 3 fields, 4 frames per field are set, and single stripe cycles in the first and second stripe are alternated during the night. The latter strategy allows a continuous coverage throughout the night, but has the disadvantage of a reduced number of fields in the declination. Figure 2-4 displays the concept with two stripes with six fields, before and after the culmination.

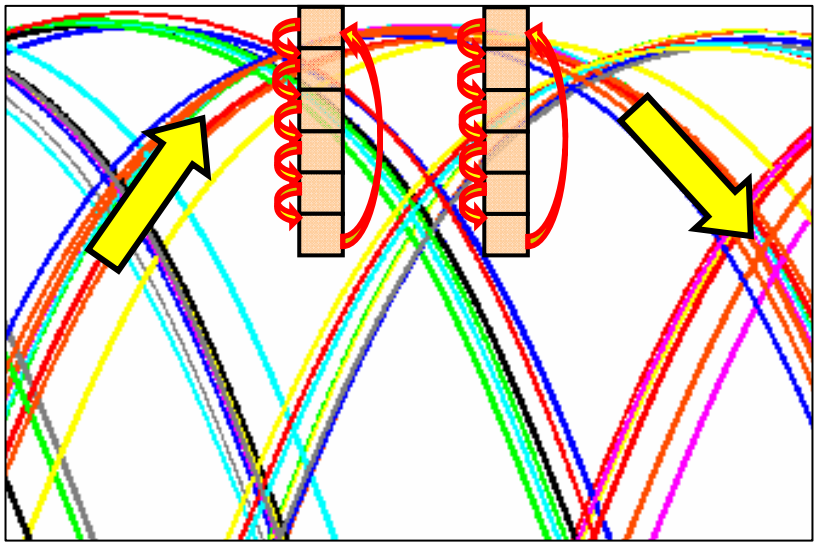

Figure 2-4: Example of 2 fences with 6 fields, symmetrically placed before and after the culmination.

2.2 Performance simulation of MEO survey strategies

Performance simulations were conducted with PROOF and with the AS4 simulator. The latter was used for the assessment of the observation strategies with different fences, where more tracklets observed at subsequent epochs need to be correlated.

2.2.1 Performance simulations with PROOF

The performance of the different pointing fields mentioned in the previous subsection was evaluated by means of the PROOF simulation tool. The parameters according to the ESASDT telescope were used for the simulations. Several PROOF runs were performed using the synthetic population. The results show that the pointing at 51° is the most successful. However, even at 55° and 0° declination a quite elevated number of detections is present. The dwell time in the FOV is around 55-60 sec in all the cases, while the best phase angle never exceeds 90° and in general is smaller for smaller declinations. Simulations show that objects up to magnitude 18 are detectable and considering a phase angle range from between 15° and 90°, the size of the detectable objects is estimated to be around 0.5 m.

2.2.2 Performance simulations with AS4

Survey simulations with the synthetic population were performed using the AS4 simulator [RD-12][RD-13] using the parameters for the ESASDT and the ZimSMART telescope. The general idea of the scenarios follows the principles previously illustrated for fence strategies. In general observations from ZimSMART provide better results than observations from OGS. The detectability from ZimSMART is higher because of its bigger FOV, which also affects the number of measurements inside the track and the duration of the track. From the simulation results it seems that there is no apparent advantage of two-stripes strategies with respect to single-field strategies. The reason for no apparent difference between the two types of scenarios is possibly given by the algorithm used for the orbit determination. In general, the AS4 simulator has not been designed for analysing so short simulations. The scenarios with a slightly longer duration of 24 hours already provide a higher number of measurements and for a small amount of objects an improvement in the orbit determination accuracy. Regarding the orbit determination accuracy, the simulations are not very conclusive. In the scope of this work, where statistical considerations about the debris population are primarily investigated, more important is the performance in terms of detections. The single-field strategy, besides being more practicable, still provides an appreciable number of detections. Moreover a minor correlation uncertainty characterizes the orbit determination process. For a fraction of the detected objects a quite accurate orbit can be determined. In a real survey campaign the single field can possibly be extended to a single fence to increase the covered observed region.

2.3 Orbit determination and follow-up strategies

Optimum follow-up strategies in MEO for the acquisition of high quality 'secured' orbits were investigated. The 'secured' orbits should guarantee a safe recovery of the object after a few weeks. A similar analysis has been conducted for GEO and GTO objects in [RD-5][RD-6][RD-7]. Orbital elements for 100 different MEO objects were randomly generated in the ranges used for the synthetic population. The generated orbital elements were used to simulate observations and an error of $\sigma = 0.5''$ was assumed for the accuracy of the single observations. Orbits were determined using the simulated observations and compared with the original ("true") orbits in order to study the accuracy of the orbit determination. The differences are given by an average $\Delta = \arccos\left(\sin\delta_t \sin\delta_d + \cos\delta_t \cos\delta_d \cos\Delta\alpha\right)$, where δ_t and δ_d are the declinations belonging to the original and the determined orbit, respectively, and $\Delta\alpha$ is the difference in right ascension α. The results show that after two/three follow-up observations during the same night the determined orbit has a sufficient accuracy for the successful recovery of the discovered MEO objects in the subsequent nights, i.e. the difference Δ remains smaller than the FOV of the ESASDT telescope (Figure 2-5). In general, the arc covered by the observations should be few hours long for a reliable orbit determination and "secured" orbit determined based on observation arcs of few days can be used to build up a catalogue. The choice of the follow-up strategy right after the discovery is important for all the subsequent recoveries. Simulations with different discovery positions and, consequently, other observation geometries, show clear differences and disclose that the above considerations cover one of many possible scenarios. Nevertheless, the results represent a valid starting point for more specific scenarios.

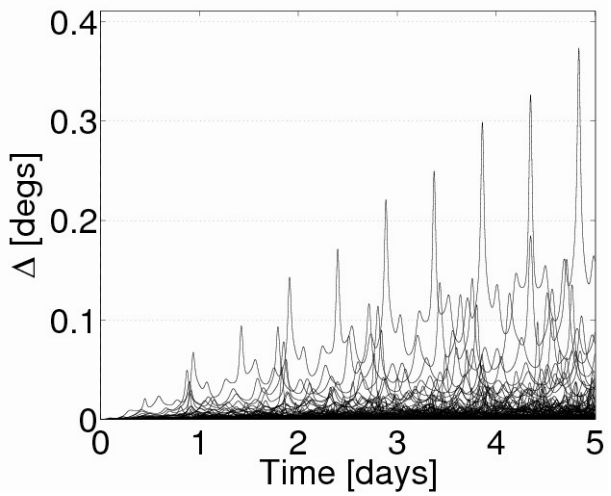

Figure 2-5: Difference Δ between "true" and elliptical orbit after 3 follow-up's during one day. After several days the difference is still smaller than the ESASDT field of view.

3 SOFTWARE REVIEW AND ADAPTATIONS

3.1 Software architecture critical review

Within the context of a future European Space Surveillance System the existing and newly developed sensors will be part of a network of sensors. Thus the information system architecture will have to evolve towards a more open and standard architecture providing interoperability between the different actors of the system. The proposed architecture, in addition to separate clearly the Service Providers from the Sensors, introduces a Data Broker actor between the Service Providers and the Sensors to be able to communalize the observations of the same object requested by different Service Providers. It keeps however the possibility for a Service Provider to have a direct link (direct request) to a sensor in case a specific relationship exists between both (e.g. the Service Provider is also the owner of the Sensor, or it is allowed by the Service License Agreement). The four types of users are:

- The **Sensor Operator** is in charge of the sensor operations like sensor planning, data acquisition and level-1 processing, quality controls and delivery. He is also in charge of the sensor maintenance and informs the Broker of the sensor status.
- The **Data Broker** is the interface between the Service Provider and the Sensors. His main task is to fulfill request from the Service Providers by tasking the most efficiently all the sensors he is managing. In the current situation, AIUB is currently behaving like a data broker by tasking several sensor (ZIMLAT, Tenerife)
- The **Service Provider** is in front of the End-User. He provides high added value services for the End-User and request data (raw acquisition, transformed ones) from the Broker. His main expertise is in the data application and related business management

- The **End-User** will request thematic services in the field of space surveillance. Each of them is associated with a specific module. Operationally speaking, these roles can be handled by one or more companies/institution.

3.2 Adaptation of Planning Tool

The Planning Tool was conceived primarily to plan survey and follow-up observations for objects in GEO and GTO orbits. Survey fields are defined by means of a graphical user interface, the so-called survey field definition panel. The geocentric positions of the survey fields are represented by straight stripes in a polar diagram showing the orbital poles of catalogued orbits of TLE and debris objects. This representation was restricted to 18° inclination for the orbital planes or 18° geocentric declination for the survey fields, respectively. This restriction was eliminated by implementing a selectable maximum inclination for the graphical display. Technically this required a major redesign and the implementation of the correct gnomonic projection instead of a simple polar diagram with linear radial scale (for declinations <20° this approximation was fully justified). Together with this enlarged inclination range a new zooming and planning function was implemented.

The survey definition allows for so-called “blind tracking” (also called “rate tracking”) during the exposures. The velocity components had to be given in the terms of so-called coordinate velocities, i.e. in the intrinsic velocities of the telescope axes. A new option to define the tracking velocities in sky motion was thus implemented.

3.3 Correlation algorithm

The observation data acquired at OGS are processed using the so-called Online/Offline Data Processing System (ODPS). In the context of this study, with the observation of higher inclined orbits, a different correlation algorithm in the ODPS system at prototype stage was used [RD-8]. At first two random object images on consecutive frames are correlated. Then the absolute value of the velocity and the direction of the velocity vector in so-called normal coordinates in the tangent plane are calculated for the presumed object represented by these two images. In the next step all preceding and all subsequent frames are checked for additional object images, which would, when combined with the first two object images, represent an object with a constant apparent direction of movement and constant apparent absolute velocity. When only two object images can be correlated, the correlation is only valid if a certain drift and pseudo-inclination limit are met and a certain number of gaps is not exceeded. Excluded from the latter condition are correlations of two images close to the limiting signal-to-noise ratio. The improved algorithm strongly reduces the probability of wrong correlations, it tolerates the presence of missing images (gaps), and it allows the correlation for objects with high inclined orbits and drift rates as long as at least three object images are available.

4 THE MEO SURVEYS AT THE ESASDT

From January 2010 to November 2010, 284 survey observations (11 minutes each) on 44 nights were performed. This corresponds to approximately 52 hours of observations. All surveys in MEO have been performed in orbit planes around GPS and GLONASS constellations.

The selection of the survey fields was done mostly considering the culmination coordinates of visible satellites. We chose the culmination point because the positions of the satellites at the culmination point are more "compact" and potentially more objects would be visible in one single survey field. Furthermore the object velocity component in declination vanishes, which makes easier the blind tracking. Based on real satellite orbits the surveys fields were planned at the topocentric culmination coordinates and half an hour later. Moreover fields above and below the culmination point (fence) were planned.

During the MEO survey campaigns no new object was found. Nevertheless, from the observed fields and the survey duration per field, and assuming the previously considered explosion population it is possible to hazard statistical considerations about the real debris population in the MEO region. The observed fields in RA / DE correlate to regions in the inclination / RAAN space as described in Figure 2-3. These regions in turn determine the number of objects of the hypothetical population that can be detected. The number is related to the volume defined by the section of the two-dimensional normal distribution of the population delimited by the FOV of the telescope (Figure 4-1). In theory, if a field at the culmination point is observed for enough long time (longer than the mean revolution time of the population) all objects, whose orbit inclination is contained in a given range, can be detected. Unfortunately the surveys do not cover in general the whole revolution period, but only discontinuous time intervals. The diagram in Figure 4-2 approximately shows the coverage during one survey in terms of number of fields observed. With the assumption of a 70 s dwell time, a 10 minutes survey on one field, since the objects have moved in the mean time, correspond to the equivalent of 8.5 fields. On the other hand the total number of observable fields in one inclination stripe is 360 deg / 0.7 deg = 514.

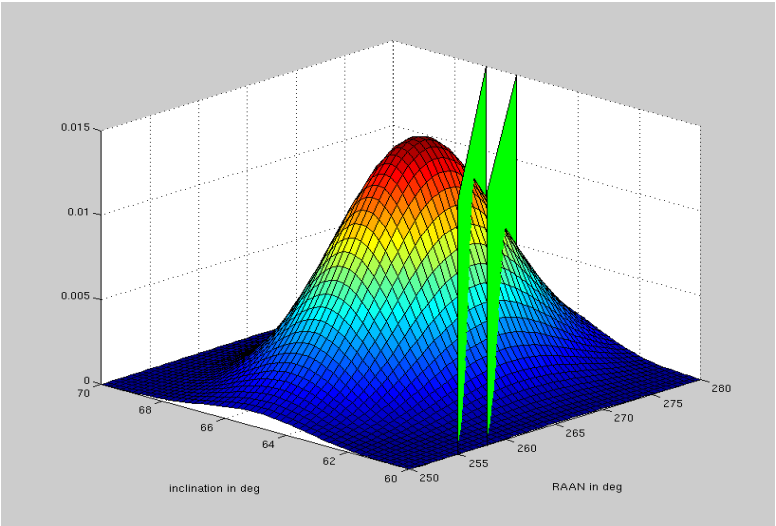

Figure 4-1: Volume of the population distribution delimited by the FOV.

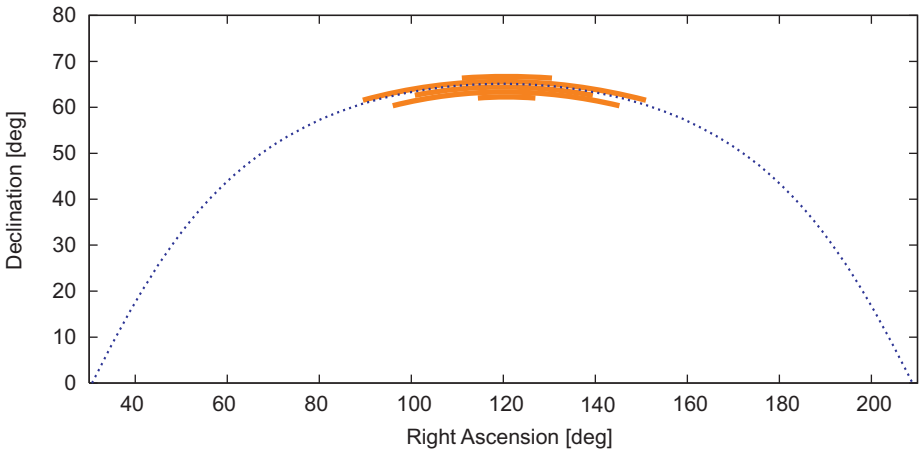

Figure 4-2: Simplified representation of the number of observed fields around a nominal GLONASS orbital plane.

The statistical problem is similar to the classical distribution of k successes in a sequence of n independent yes/no experiments, each of which yields success with probability p. In statistics the problem is described by the binomial distribution. Applied to our surveys, k = 0, since no new object was found, n is the number of observed fields, and p is the searched probability. The common estimator p' for the binomial distribution yields p' = k/n = 0. More useful is to determine a confidence interval $[p_l, p_u]$ with a lower limit p_l and an upper limit p_u around p'. For a 95% confidence level with k = 0, the lower limit is $p_l = 0$, while p_u is determined according to the area of the distribution delimited by k. When k and n are given, and p is the unknown, it is comfortable to use one of the existing statistics tools for the calculation, e.g. the "betainv" function in the Excel software. The unknown p_u, for a 95% confidence level with k = 0, is calculated with:

$$p_u = \beta^{-1}(95\%, 1, n) .$$

The estimated upper limit, according to p_u, of number of objects present in the different groups of the GPS/GLONASS constellations depends obviously on the number of fields covered. Very few observations were conducted in the GPS constellations and no conclusive results were obtained, whereas for the GLONASS constellations the upper limit varies between 10 and 40 objects. If we recall the fragment distribution (Figure 2-1) in the explosion model discussed previously, we can expect around 200 objects with a limiting size for the ESASDT of 20 cm. This might lead with some precaution to the statement that no explosion has occurred at least in the examined GLONASS orbits. On the other hand, the model is based on assumptions on the explosion process and on the propagation of the debris fragments, thus it might not thoroughly reflect the real conditions.

5 GEO/GTO SURVEYS AT THE ESASDT

5.1 The observation campaigns

In addition to MEO surveys, routine space debris surveys and catalogue maintenance observations were performed in 2009 and 2010 at OGS. The campaigns consisted of a mixture of GEO and GTO surveys – a continuation of the work performed in the ESA Contracts 17825/03/D/HK, "Space Debris Optical Observations and Analysis with ESA's 1m Telescope" – as well as follow-up observations of newly detected objects and of catalogued objects. A limited set of follow-up observations of newly detected, uncatalogued objects was acquired during the surveys. The aim of these observations was primarily to allow for the determination of elliptical orbits for a sample of the objects. After a successful 6-parameter orbit determination the new object was added to the internal ESA/AIUB catalogue. Table 5-1 gives an overview of all the ESA GEO and GTO campaigns from 2005 until 2010. The terms 'correlated' and 'uncorrelated' refer to objects/detections for which a corresponding catalogue (ESA DISCOS) object could or could not be identified, respectively. Some of the detections may actually refer to the same object, i.e., we may have incidentally re-observed some of the objects previously. We subsume all detections that seem to belong to the same real object under the term 'correlated object'. 'Uncorrelated detections' are detections that cannot be identified with known objects of the DISCOS catalogue.

	Jan – Dec 2005 GEO/GTO	Jan – Dec 2006 GEO/GTO	Jan – Dec 2007 GEO/GTO	Jan – Dec 2008 GEO/GTO	Jan – Dec 2009 GEO/GTO	Jan – Dec 2010 GEO/GTO
Frames	59'500	70'000	56'000	48'700	57'600	26'600
Scanned Area	8'800 deg^2	9'800 deg^2	7'600 deg^2	6'480 deg^2	7'320 deg^2	2'620 deg^2
Total Observation Time	**85 nights / 495 h**	**95 nights / 580 h**	**81 nights / 461 h**	**78 nights / 399 h**	**96 nights / 478 h**	**71 nights / 212 h**
GTO / Follow	**205 h/141 h**	**234 h/216 h**	**180 h/193 h**	**117 h/194 h**	**149 h/246 h**	**19 h/175 h**
Correlated detections	708	808	483	319	414	130
Correlated objects	443	288	241	196	216	91
Uncorrelated detections	**922**	**1040**	**618**	**403**	**274**	**67**

Table 5-1: GEO and GTO campaigns from 2005 to 2010.

5.2 AIUB/ESA catalogue

The AIUB/ESA catalogue as of June 2011 contains 1172 uncorrelated small-size objects in GEO, GTO and GEO-like orbits for which 6-parameter orbits were determined. Figure 5-1 shows the inclination vs. RAAN diagram of observed objects from 2002 to June 2011. Some distinct debris clouds in the (Ω, i)-space can be seen in the data from all years. The evolution of the orbits of these clouds can be monitored closely and compared with theoretical models. The only rational explanation for the origin of these clouds is breakup events.

For 318 objects of the catalogue the AMR could be determined and it was found that there is a significant population of objects with AMR larger than 1 m^2/kg. A closer analysis reveals that the majority of the objects with AMR larger than 1 m^2/kg are objects with a mean motion near 1 rev/day and eccentricities ranging from 0.05 to 0.8. In Figure 5-2, which shows the eccentricity as a function of the mean motion for the objects of the AIUB/ESA catalogue, this population is the vertically dispersed cloud concentrated at a mean motion of 1 rev/day.

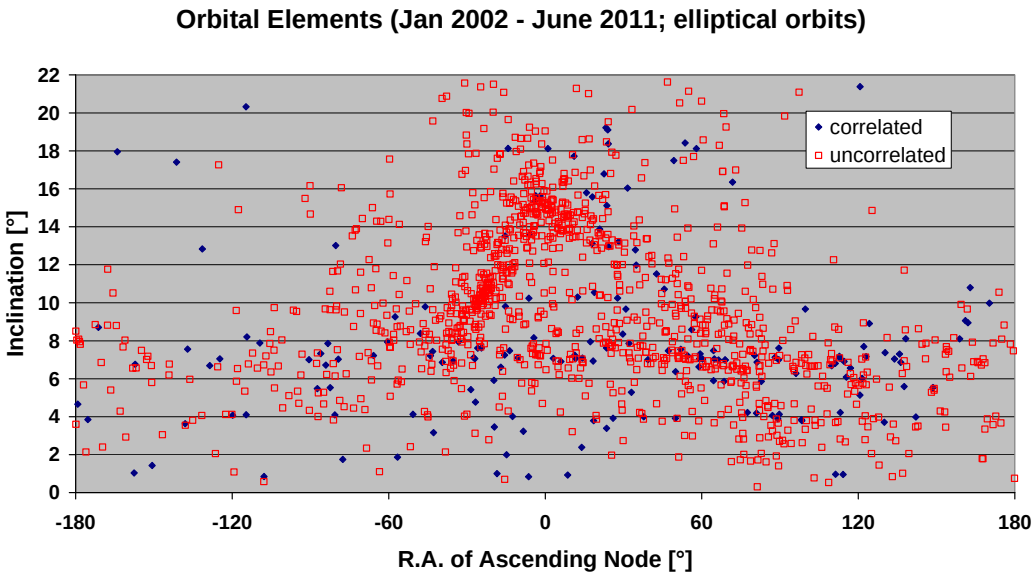

Figure 5-1: Inclination vs. right ascension of ascending node of observed objects from 2002 to June 2011.

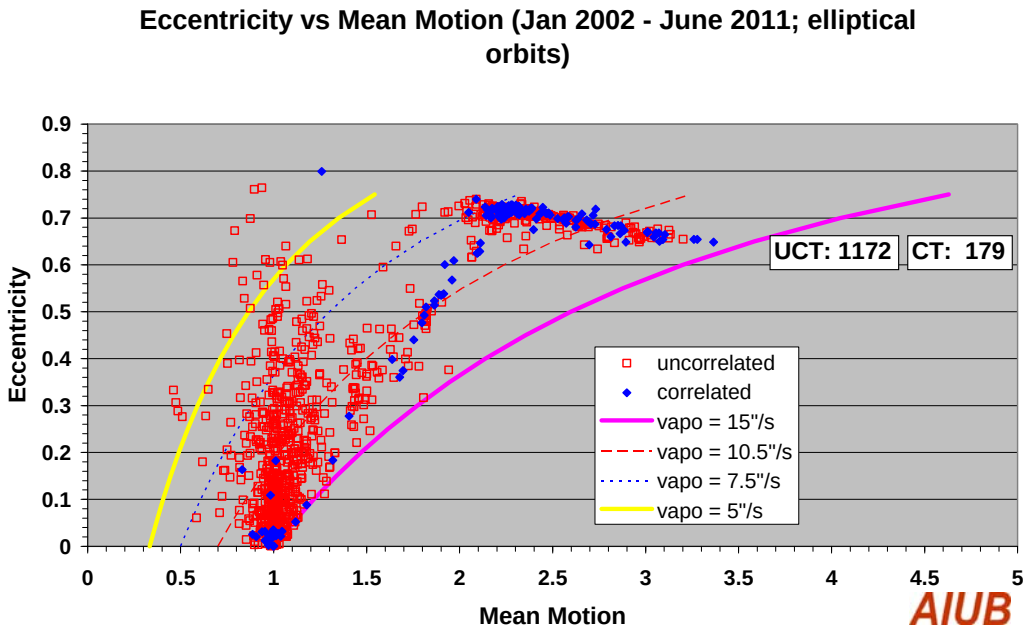

Figure 5-2: Eccentricity as a function of the mean motion of 1172 uncorrelated and 179 correlated objects for which 6-parameter orbits were determined.

6 SUMMARY AND CONCLUSIONS

6.1 Summary and conclusions

The main goal in this study was the development of strategies for the observation of space objects in the MEO region and the subsequent characterization of the space environment in that region. It was decided to concentrate the analysis in terms of "space debris measurement", rather than "space surveillance". In the former the research focuses on acquisition and interpretation of data describing the characteristics of space debris objects in a given survey volume in a more statistical manner. The space debris surveys must be designed such that they yield a statistically well-defined sample of the space debris population in a given orbit region. Due to the dependence on different observation parameters, like e.g. sensitivity and blind tracking, in most cases the surveys are optimized for different sub-regions of the orbital element space. Several survey strategies have been studied taking into account the different ESASDT telescope parameters and a synthetic object population. Starting with a reference population of known objects taken from the DISCOS TLE catalogue, the distribution of fragments after a possible explosion and the evolution of the orbital elements after 55 years have been simulated. A synthetic population of 1000 objects around the nominal values for the GPS and GLONASS constellations was created. Based on this population the best possible survey regions with high detection rates were estimated. Using a simple geometrical model considering the GPS/GLONASS constellations the main regions were identified, among other at the orbit culmination and at the orbital node. However, of the possible solutions the obser-

vation at the culmination point was preferred since it offered the advantage of only one blind tracking direction. In general, to exhaustively cover a certain sky region the observation strategy needs to consider the FOV of the sensor and the dwell time of MEO objects in the given FOV. Depending on the dwell time and the observation cycle (exposure, readout, new telescope pointing), a multiple fences strategy can be conceived. However in the case of the ESASDT telescope, with a FOV of 0.7° and a cycle time of 22 s, only a single field strategy was chosen. Performance simulations of the single field strategies were conducted with PROOF, whereas the AS4 simulator was mainly used for the assessment of the observation strategies with different fences, where more tracklets observed at subsequent epochs need to be correlated. PROOF simulations confirmed the detectability of the objects depending on phase angle and apparent magnitude in the analyzed strategies. The AS4 simulations showed a slightly improvement in the orbit determination for fence scenarios with different re-observations intervals, but the results are not very conclusive. According to the simulations the single-field strategy, besides being more suitable for the processing of the ESASDT data, still provides an appreciable number of detections.

Besides survey strategies, follow-up scenarios were investigated for the maintenance of the orbital data of new discovered objects. The results show that after two follow-up observations during the same night the determined orbit has a sufficient accuracy for the successful recovery of the newly detected MEO objects in the subsequent nights. As emerged from the simulations, the influence of the time intervals of the first and second follow-up, as well as the discovery position and the observation geometry are crucial for the optimization of the strategy.

A critical review of the software architecture used at the ESASDT telescope was performed. The proposed architecture in the context of a network of sensors goes towards a more open and standard architecture providing interoperability between the different actors of the system, like Service Providers, Sensors, and Data Brokers. Furthermore, adaptations to the current software were done to extend the observation planning capabilities and to allow the detection of objects on highly inclined orbits.

In the experimental part of the study, routine surveys and follow-ups were conducted, providing statistics about the GEO/GTO and high area-to-mass population, and allowing the object catalogue maintenance. Additionally, 284 surveys (11 minutes each) in the MEO region on 44 nights have been performed from January 2010 to November 2010. Most of the observations were executed around the culmination of the nominal GPS and GLONASS orbits. Since no new object was discovered during the observation campaigns, the data were analyzed with a statistical approach. The problem with the number of found objects in a number of observed fields was evaluated in a similar way to the classical binomial distribution, which describes the number of successes in a sequence of independent yes/no experiments, each of which yields success with a certain probability. With a 95% confidence level it was possible to determine an upper limit for the estimated number of objects around the investigated orbital planes. Based on these estimates and on the assumptions for the explosion population, the results lead with some precaution to the statement that no explosion has occurred in the examined orbits.

6.2 Recommendations

During this study the efforts were concentrated on the characterization of the MEO environment from a statistical point of view. The approach adopted based on the assumption that at

some point in time somewhere in the MEO region one or more explosions occurred. The latter is a strong assumption that does not cover all the possible mechanisms responsible for the production of debris. Other models including different sources of fragmentation, e.g. delamination, should be considered.

The AS4 simulations of different survey scenarios have shown several promising strategies to cover MEO regions occupied by GPS and GLONASS constellations. Simulations over relative short intervals (several observations within the same night) were conducted to investigate especially the detection and re-observing capabilities. However, the strategies should be simulated over longer time intervals in order to fully exploit the potential of the AS4 simulator. On the other hand, the simulated survey-only strategies are for the moment not applied in the OGS campaigns because a tracklet correlation algorithm in the data processing system is not available. In this direction further development should be done.

The simulations of follow-up strategies indicate a general approach to apply in order to recover discovered objects and eventually to catalogue them. In a further step the strategies could be optimized according to the specific orbit of the discovered object. The optimization should ensure a high quality orbit with a minimum of re-observations.

The algorithm to correlate observations to single tracklets has been extended to fit orbits in the interested MEO region. Still, the definition of the parameters could be generalized for any type of orbit, object velocity, or specific range.

The survey campaigns at OGS have provided indications on the real debris population in orbit planes around GPS/GLONASS constellations. However, the results base on statistical considerations and a more exhaustive coverage of the interested regions is strongly suggested. This would imply a larger number of survey fields, alternatively larger telescope sensitivity or field of view.

7 REFERENCES

[RD-1] Donath, Th., T. Schildknecht, P. Brousse, J. Laycock, T. Michal, P. Ameline, L. Leushacke, 'Detailed Assessment of a European Space Surveillance System', Final Report ESA/ESOC Contract 18574/04/D/HK(SC), 2005.

[RD-2] Pardini, C., L. Anselmo, 'Dynamical evolution of debris clouds in geosynchronous orbit', Advances in Space Research 35, pp. 1303-1312, 2005

[RD-3] G. Beutler, 'Methods of Celestial Mechanics', 2 Volumes, Springer 2005.

[RD-4] Program for Radar and Optical Observation Forecasting (PROOF), Final Report, ESOC Contract 18014/03/D/HK(SC), 2006

[RD-5] Musci, R., T. Schildknecht, M. Ploner, 'Orbit improvement for GEO objects using follow-up observations', Advances in Space Research 34, pp. 912-916, 2004

[RD-6] Musci, R., T. Schildknecht, M. Ploner, G. Beutler, 'Orbit improvement for GTO objects using follow-up observations', Advances in Space Research 35, pp. 1236-1242, 2005

[RD-7] Musci, R., T. Schildknecht, G. Beutler, V. Agapov, ‚Observations of high altitude objects from multiple sites', Proceedings of the International Astronautical Congress IAC-06-B6, 2006

[RD-8] Früh, C., R. Musci, T. Schildknecht, 'Improved method for recognizing unknown space debris objects on series of CCD-Frames", Proceedings of the International Astronautical Congress IAC-08-A6, 2008

[RD-9] Schildknecht, T., R. Musci, M. Ploner, W. Flury, J. Kuusela, J. de Leon Cruz, and L. de Fatima Dominguez Palmero, 'An Optical Search for Small-Size Debris in GEO and GTO', AMOS Technical Conference, September 9-12, Maui, Hawaii, 2003.

[RD-10] Schildknecht, T., R. Musci, W. Flury, J. Kuusela, J. de Leon Cruz, and L. de Fatima Dominguez Palmero, 'Optical Observations of Space Debris in High-Altitude Orbits', Proceedings of the Forth European Conference on Space Debris, pp. 113-118, ESOC, Darmstadt, Germany, 18-20 April 2005.

[RD-11] Schildknecht, T., R. Musci, T. Flohrer, 'Properties of the High Area-to-mass Ratio Space Debris Population at High Altitudes', Advances in Space Research Vol. 41, pp 1039–1045, 2008.

[RD-12] 'Advanced Space Surveillance System Simulator', Final Report of ESOC Contract No.18687/04/D/HK (SC), DEIMOS Space S.L, March, 2006

[RD-13] 'Design and development of Space Surveillance System Catalogue Correlation Techniques', Final Report of ESOC Contract No. 20070/06/NL/H6, DEIMOS Space S.L, December, 2007